Available online at www.sciencedirect.com

SciVerse ScienceDirect

Ceramics International 39 (2013) 3173–3181

CERAMICS INTERNATIONAL

www.elsevier.com/locate/ceramint

# Synthesis and characterization of hierarchical ZnS architectures based nanoparticles in the presence of thioglycolic acid

Maryam Mohammadikish[a,*], Fatemeh Davar[b], Mohammad Reza Loghman-Estarki[c], Zohreh Hamidi[a]

[a]Department of Chemistry, Faculty of Sciences, Kermanshah Branch, Islamic Azad University, Kermanshah, Islamic Republic of Iran
[b]Faculty of Chemistry, Razi University, Kermanshah, P. O. Box. 671441-4671, Islamic Republic of Iran
[c]Department of Materials Engineering, Isfahan University of Technology, Isfahan, Islamic Republic of Iran

Received 30 July 2012; received in revised form 28 September 2012; accepted 1 October 2012
Available online 29 October 2012

**Abstract**

Spherical ZnS based nanoparticles (hierarchical architectures) were successfully synthesized using Zinc bis(salicyle aldehitato), $Zn(Sal)_2$, thioacetamide (TAA) and thioglycolic acid (TGA) as $Zn^{2+}$, sulfur source and capping agent, respectively. The hierarchical ZnS structure was produced from the self-assembly of nanoparticles with diameters of $21 \pm 4$ nm. The products were characterized by X-ray diffraction (XRD), scanning electron microscopy (SEM), transmission electron microscopy (TEM), selected area electron diffraction (SAED), and Fourier transform infrared (FT-IR) spectra. The influence of temperature on the morphology of the products was also investigated. The possible formation mechanism and optical properties of these architectures were also reported.


*Keywords:* Optical properties; Nanostructures; Zinc blende; ZnS nanocluster

## 1. Introduction

Zinc Sulfide, an II–VI semiconductor with a direct bandgap of 3.5–3.7 for cubic and 3.7–3.8 eV for hexagonal phase, is considered as a versatile semiconductor material with exceptional physical and chemical properties. It has been extensively investigated due to its potential applications in optics, photoelectronics, sensors, catalysts and so on [1–4]. In recent years, numerous efforts have been made to control the fabrication of nanostructured materials with various morphologies, since the novel properties and potential applications of nanomaterials depend largely on their shapes and sizes [1].

The complex 3D architectures constructed by 1D and 0D nanostructure show unique properties different from those of the mono-morphological structures because of combining the features of nanoscale building blocks [4]. Efforts were devoted to the self-assembly of nanoscale building blocks into complex 3D architectures such as hierarchical ZnS hollow superstructures, sea urchin-like ZnS nanostructures and ZnS nanoflower [5–8]. Up to now, considerable efforts have been devoted to synthesize ZnS nanostructures. A large number of ZnS nanostructures with simple morphologies, such as thin film, nanowires, and nanorods have been prepared by various techniques [8–12]. However, the successful synthesis of ZnS nanostructures with complex 3D architectures is difficult and rarely reported. In addition, most methods for the synthesis of ZnS nanostructures, such as the single-source molecular precursor, chemical vapor deposition (CVD) method and the $\gamma$-irradiation route demand vacuum techniques, high temperature, or complicated controlling processes, which are unfavorable for low-cost and large-scale production. Therefore, it is of great importance and necessity to develop a facile technique to synthesize ZnS with complex 3D architectures in mild conditions.

The use of the coating in hydrothermal method is known to yield excellent results. There are some reports showing thioglycolic acid as an appropriate capping agent for the

*Corresponding author. Tel./fax: +98 831 725 2218.
*E-mail address:* mohammadikish@iauksh.ac.ir (M. Mohammadikish).

0272-8842/$ - see front matter © 2012 Elsevier Ltd and Techna Group S.r.l. All rights reserved.
http://dx.doi.org/10.1016/j.ceramint.2012.10.001

synthesis of ZnS nanostructures in hydrothermal process. Yang's groups had developed a mild hydrothermal route to synthesize metal sulfides using thioglycolic acids as nontoxic template [13]. Xue and Yan successfully synthesized ZnO/ZnS nanocable and ZnS nanotube arrays via thioglycolic acid and $Na_2S$ [14]. Qian's group has also synthesized new ZnS/organic composite nanoribbons with the use of thioglycolic acid [15].

Our strategy has been to use a thioglycolic acid as capping agent for hydrothermal synthesis of spherical ZnS based nanoparticles (hierarchical architectures). It still remains a great challenge to develop facile and environmentally benign methods for creating ZnS nanostructures from a simple precursor. A major interest at the moment is in the development of organometallic or inorganic compound for the preparation of nanostructures. Using the novel compounds can help open a new way for preparing nanomaterials to control nanoparticle size, shape and distribution size. In this paper, we report a facile hydrothermal method for the preparation of ZnS hierarchical architectures using $Zn(Sal)_2$, thioacetamide and TGA as $Zn^{2+}$, sulfur source and capping agent, respectively. The morphologies and structure of the products were studied by FESEM, XRD and TEM. The influence of temperatures on the morphology of the products was investigated. Possible formation mechanism and optical properties of these nanoflowers were also reported.

## 2. Experimental

### 2.1. Materials and characterization equipment

All the chemicals were of analytical grade and used as received without further purification. XRD patterns were recorded by a Rigaku D-max C III, X-ray diffractometer using Ni-filtered Cu Kα radiation. Field emission scanning electron microscopy (FESEM) images were obtained on Hitachi (Japan). Transmission electron microscopy (TEM) and Electron diffractions (SAED) images were obtained on a Philips (EM 208 and CM 30) transmission electron microscope with an accelerating voltage of 100 kV (EM 208) and 250 kV(CM30 model). Fourier transform infrared (FT-IR) spectra were recorded on Rayleigh WQF-510 spectrophotometer in KBr pellets. The electronic spectra of the complexes were taken on a Bio UV–visible spectrometer (Varian Cary 100). Particle sizes (Dc) were calculated from the line broadening of the X-ray diffraction peaks using the Debey–Scherrer Eq. (1) [1,3]:

$$Dc = k\lambda/\beta\cos\theta \quad (1)$$

where $\beta$ is the breadth of the observed diffraction line at its half-intensity maximum, $k$ is the so-called shape factor, which usually takes a value of about 0.9, and $\lambda$ is the wavelength of X-ray source used in XRD.

### 2.2. Preparation of spherical ZnS based nanoparticles

In a typical synthesis, 0.52 g of $Zn(Sal)_2$ powder is dissolved in 100 ml of distilled water and 1.1 mL of thioglycolic acid (TGA) with the concentration of 0.056 M was mixed slowly under stirring. After 10 min stirring, stoichiometric amount of thioacetamide (TAA) as the sulfur source was introduced into the aforementioned solution, which was then transferred into Teflon lined stainless steel autoclave with 300 mL capacity, sealed and maintained at 110–200 °C for 6 h. Subsequently, the resulting white solid product was centrifugalized, washed

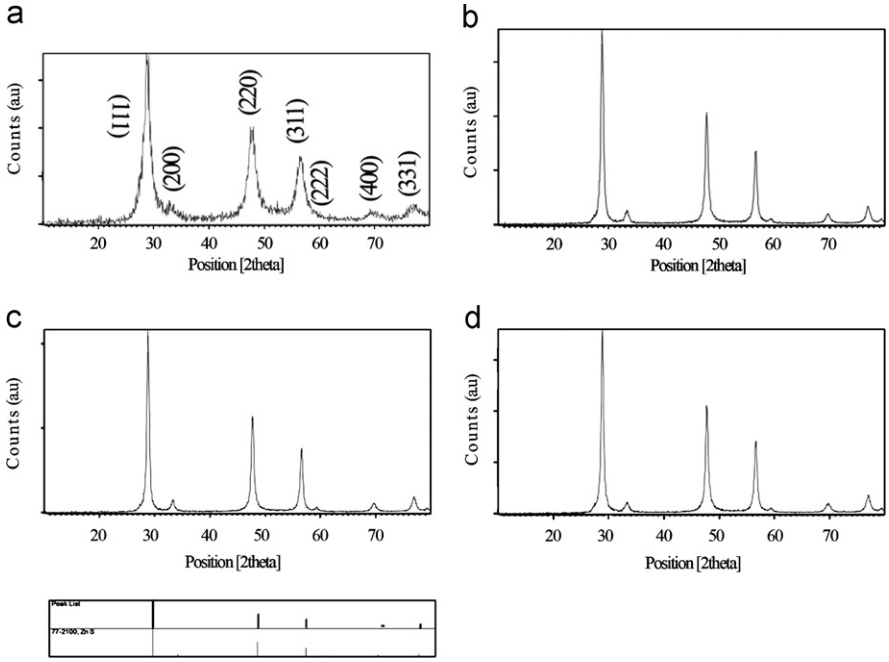


Fig. 1. XRD patterns of as-prepared samples at different temperatures for 6 h (a) 110 °C, (b) 140 °C, (c) 160 °C and (d) 200 °C.

with distilled water and ethanol to remove the ions possibly remaining in the final product and finally dried at 50 °C in air.

## 3. Results and discussion

### 3.1. XRD patterns

Fig. 1 shows the powder X-ray diffraction patterns of the resultant products obtained at different temperatures. All of the products displayed the XRD peaks corresponding to cubic (JCPDS No. 77-2100) zinc blende (sphalerite) and no characteristic diffraction peaks arising from the possible impurity phases such as TGA, S, ZnO, etc., were observed, indicating the preparation of pure cubic sphalerite samples by the hydrothermal route. The average calculated dimensions along [111], [220], [311], [400] and [331] from FWHM (full width at half of maximum) are depicted in Table 1. According to Scherrer's equation [1,3], the crystallinity and sizes of the resultant products were customarily enhanced with varying the reaction temperature. Using the Scherer equation, it could be seen that the growth of crystallite size was slow at 110 °C, but, between 140–200 °C, there is a significant grain growth and better crystallinity, as compared with the reaction at temperature 110 °C.

### 3.2. SEM images

Fig. 2 shows SEM images of as-produced powder at different temperatures. SEM images depict almost the products (Fig. 2a–h) prepared by $Zn(Sal)_2$ at 110, 140, 160, 200 °C. They consist of a spherical morphology with diameter of 400–500 nm. Furthermore, it was seen that with increasing reaction temperatures from 110 °C to 200 °C, some nanospheres were broken to smaller spherical particles (Fig. 2g and h). A close look at Fig. 2a–h shows the spherical morphology produced from the self-assembly of nanoparticles with 30–40 nm diameters. It can be seen from Fig. 2c–e that the nanospheres were hollow. The rough surface of sphere is actually the manifestation of the self-assembly of particle. It should be noted that the semispherical nanoparticles on the sphere can be seen in the FESEM image. The formation mechanism for it will be discussed elsewhere. Interestingly, when the zinc acetate, $Zn(AC)_2$, was used as the $Zn^{2+}$ source instead of $Zn(Sal)_2$, in the TGA-assisted hydrothermal process, the obtained product of ZnS was rod-like particles [8] and they were not spherical based nanoparticles.

Table 1
Crystallite size of as-prepared product at different temperatures.

| Temperatures (°C) | FWHM of (111) | Crystallite size (nm) | Average Crys. size (nm) |
|---|---|---|---|
| 110 | 0.6888 | 11.9 | 8.64 |
| 140 | 0.4133 | 19.9 | 19.3 |
| 160 | 0.3542 | 23.2 | 20.5 |
| 200 | 0.4133 | 19.9 | 24.4 |

### 3.3. TEM and SAED image

The typical TEM and SAED images of the as-prepared product at 110 °C and 200 °C are shown in Fig. 3. As revealed by the SEM image (Fig. 2), the TEM images (Fig. 3b) again illustrate that the ZnS sphere consists of a few nanoparticles. According to TEM image (Fig. 3a), the diameter of the sphere was more than 500 nm. As can be seen in Fig. 3a, the spheres were hollow. These results are good agreement with SEM images (Fig. 2). Fig. 3b, 3c and 3d show high magnification of the sample prepared at 110 °C and 200 °C, respectively. When reaction temperature was 110 °C, there were semispherical particles with the average size of $10 \pm 3$ nm on the nanosphere. Upon increasing reaction temperature to 200 °C, there was a significant crystal growth. A close look at Fig. 3d shows that some semispherical grew to sword-like particles with the average size of $21 \pm 2$ nm on the nanosphere. Inset Fig. 3d shows that some nanospheres were broken to nanoparticles with diameters of 30–40 nm. These results are in good agreement with XRD (Table 1) and UV–vis analysis (Table 2). From SAED of both samples synthesized at 110 °C and 200 °C (Fig. 3e and f), it was seen that ZnS nanospheres were polycrystalline and the (111), (220) and (311) planes from inside ring to the outside of SAED analysis clearly confirm the zinc blende structure of products [6]. Furthermore, according to Fig. 3e, it was seen that due to encapsulation with the organic substance (TGA), the electron diffraction rings were relatively obscure. The FTIR (Fig. 5) spectrum confirms the presence of organic molecule (TGA) on the samples synthesized at 110 °C, to be discussed later. However, when reaction temperature was 110 °C (Fig. 3e), it was clearly seen that the rings of SAED were continuous while electron diffraction rings of the sample at 200 °C (Fig. 3f) were point by point. So, this confirms that there is a crystal growth during increasing reaction temperature from 110 °C to 200 °C [16,17].

### 3.4. Formation mechanism

In order to indicate the formation mechanism for the two different nanostructures described above, a schematic diagram is depicted as Fig. 4. Prior to the hydrothermal process, a complex species of $ZnSHCH_2COOH_2^+$ shown in Fig. 4(2) was formed once the TGA was introduced into the $Zn^{2+}$ aqueous solution. When thioacetamide was introduced into the $Zn(OAC)_2$ solution, the complex ZnS clusters, i.e.$(ZnS)_m(ZnSCH_2COOH)_k^+$, as shown in Fig. 4(3), were generated. During the hydrothermal process, the organic ligand, $SCH_2COOH^-$, was dissociated from the complex ZnS clusters at certain sites, as shown in Fig. 4(5a). At these sites, as shown in Fig. 4(5b), the oriented attachment between the complex ZnS

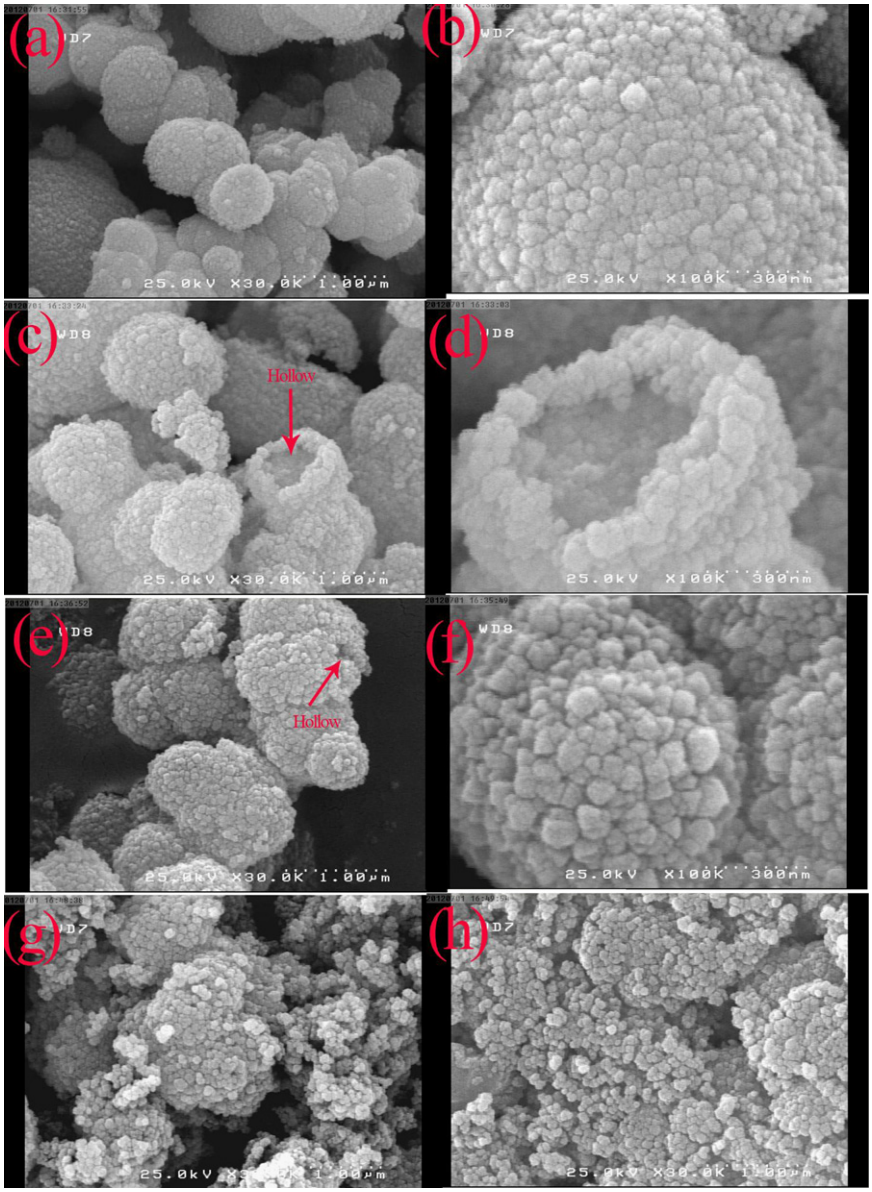


Fig. 2. SEM images of as-prepared samples with $Zn(Sal)_2$ at different temperatures for 6 h (a and b) 110 °C, (c and d) 140 °C, (e and f) 160 °C and (g and h) 200 °C.

clusters produced ultimately led to the formation of ZnS nanorods [13–15]. To summarize, the formation of ZnS nanorods in the TGA-assisted hydrothermal process using $Zn(OAC)_2$ as $Zn^{2+}$ source is via *cluster-to-cluster attachment* mechanism.

With the use of $Zn(Sal)_2$ as the $Zn^{2+}$ source, due to the steric hindrance and the TGA difficulty in linking $Zn^{2+}$ in the precursor solution, transformation of ZnS clusters to ZnS cluster complex was not possible by TGA, and the complex species of $ZnSHCH_2COOH^{2+}$ remained the same, as shown in Fig. 4. (4). Each complex ZnS cluster could grow up, leading to the formation of the complex ZnS particle. In the meantime, a part of organic ligands of $SCH_2COOH^-$ was broken away from the complex ZnS particles. Consequently, the attachment of ZnS particles that were partially capped with $SCH_2COOH^-$ occurred. The formation of spherical ZnS based nanoparticles is most likely due to the fact that the formation of complex ZnS particles and the dissociation of $SCH_2COOH^-$ proceeded simultaneously during the hydrothermal process (Fig. 4(6)). So, during the hydrothermal process, ZnS particles were combined together, producing flower-like ZnS based nanoparticles. Herein, it can be believed that the *particle-to-particle attachment* mechanism was responsible for the formation of spherical ZnS based nanoparticles [17,18].

Furthermore, TGA has been generally used as a templating micelle molecule to synthesize mesoporous material to favor the erosion of zinc and control the morphology of spherical ZnS crystals. The SEM image of the TGA capped particles confirms the formation of several distinct

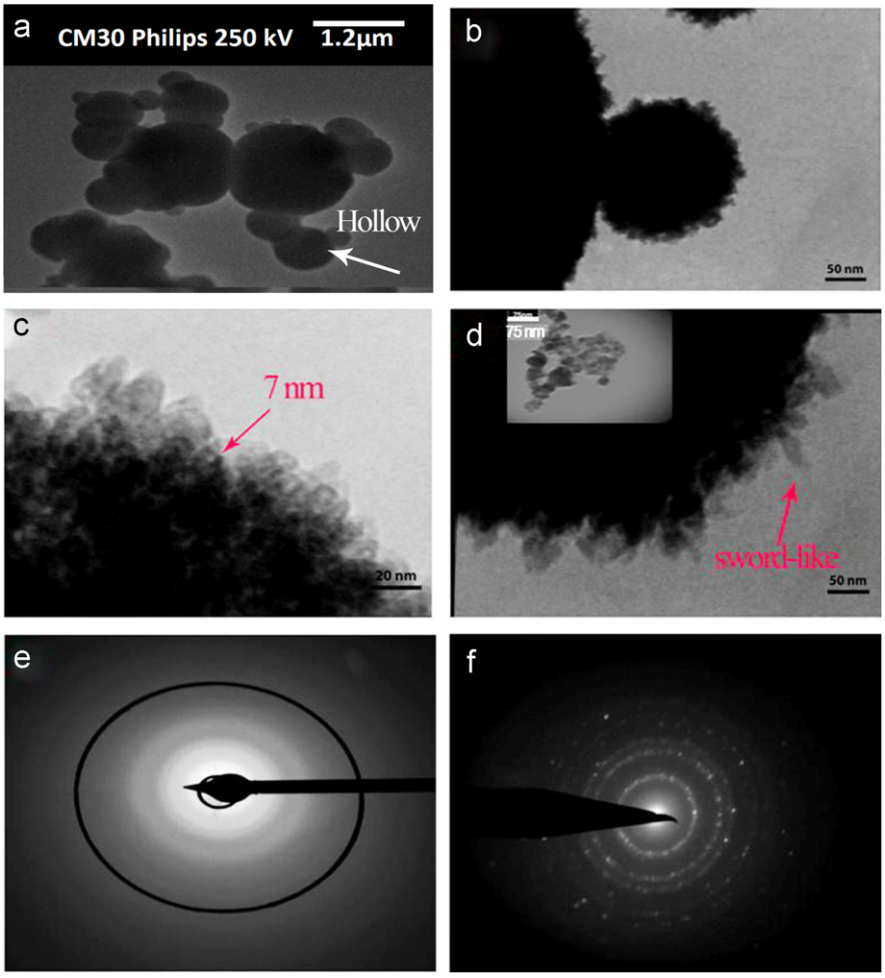


Fig. 3. (a–d) TEM images of ZnS nanosphere based nanoparticles synthesized at (a–c) 110 °C and (d) 200 °C, and (e, f) SAED images of samples at synthesized at (e) 110 °C and (f) 200 °C. White arrow show nanospheres were hallowing.

Table 2
Optical bandgap ($E_g$) and nanoparticle diameter ($d_{abs.}$) as calculated from Tauc plots and Wang equation.

| Temperatures (°C) | 110 | 140 | 160 | 200 |
|---|---|---|---|---|
| $E_g$ (eV) | 3.87 | 3.71 | 3.68 | 3.65 |
| $d_{abs}$ (nm) | 10.57 | 22.00 | 35.19 | 47.70 |
| Wavelength (nm) | 320.40 | 334.23 | 336.95 | 339.72 |

spheres. During the hydrothermal process, each complexed ZnS species can grow up and lead to the formation of spherical ZnS particle. In the mean time, a part of organic ligands $SCH_2COOH^-$ broken away from the complexed ZnS particles proceeded during the hydrothermal process.

### 3.5. FTIR spectra

Fig. 5 shows the FTIR spectra of $Zn(sal)_2$ (Fig. 5a) and samples obtained at different temperatures between 110–200 °C. In the curve (Fig. 5c–d), the typical absorbencies at 3421–3428, 1578–1601 $cm^{-1}$ and 1377–1379 $cm^{-1}$ were corresponding to –OH, and –COOH (asymmetry and symmetry stretching) functional group of the thioglygolic acid ($SHCH_2COOH$), respectively. FTIR shows that there is a small amount of capping agent (TGA) on the as-prepared product, confirming the stabilization of ZnS nanoflowers [8]. Different from pure liquid-state thioglygolic acid [8,15], the FTIR vibration peaks of ZnS obtained at 110 °C are much sharper and stronger, signaling weaker interactions and ordered arrangements of thioglygolic acid molecules existing in the reactant. This phenomenon could be explained by periodic intercalations of a relatively small amount of thioglygolic acid molecules into the inorganic frameworks composed of ZnS, which minimizes the interaction between neighboring thioglygolic

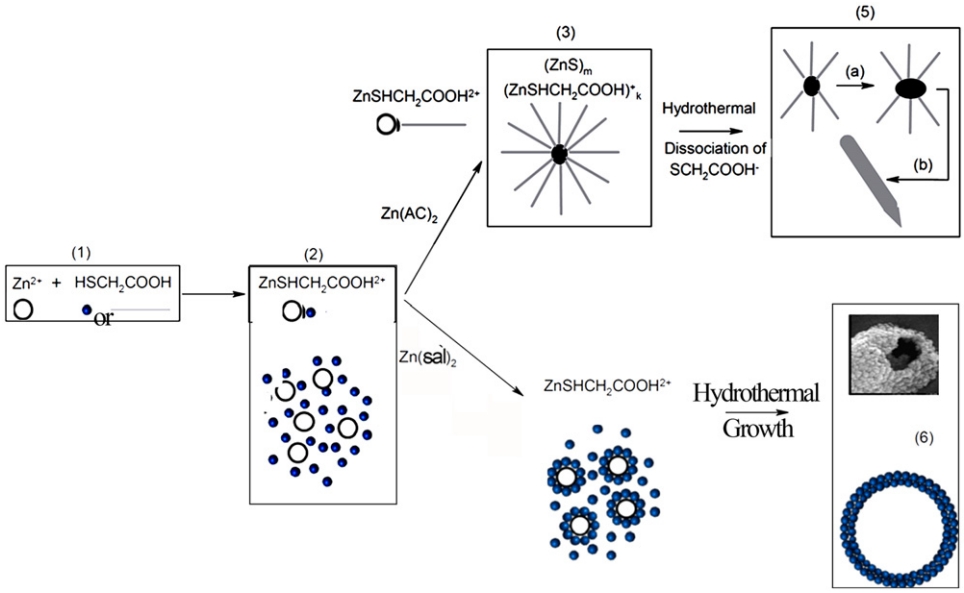


Fig. 4. Schematic of probable formation mechanism of ZnS nanosphere based nanoparticles.

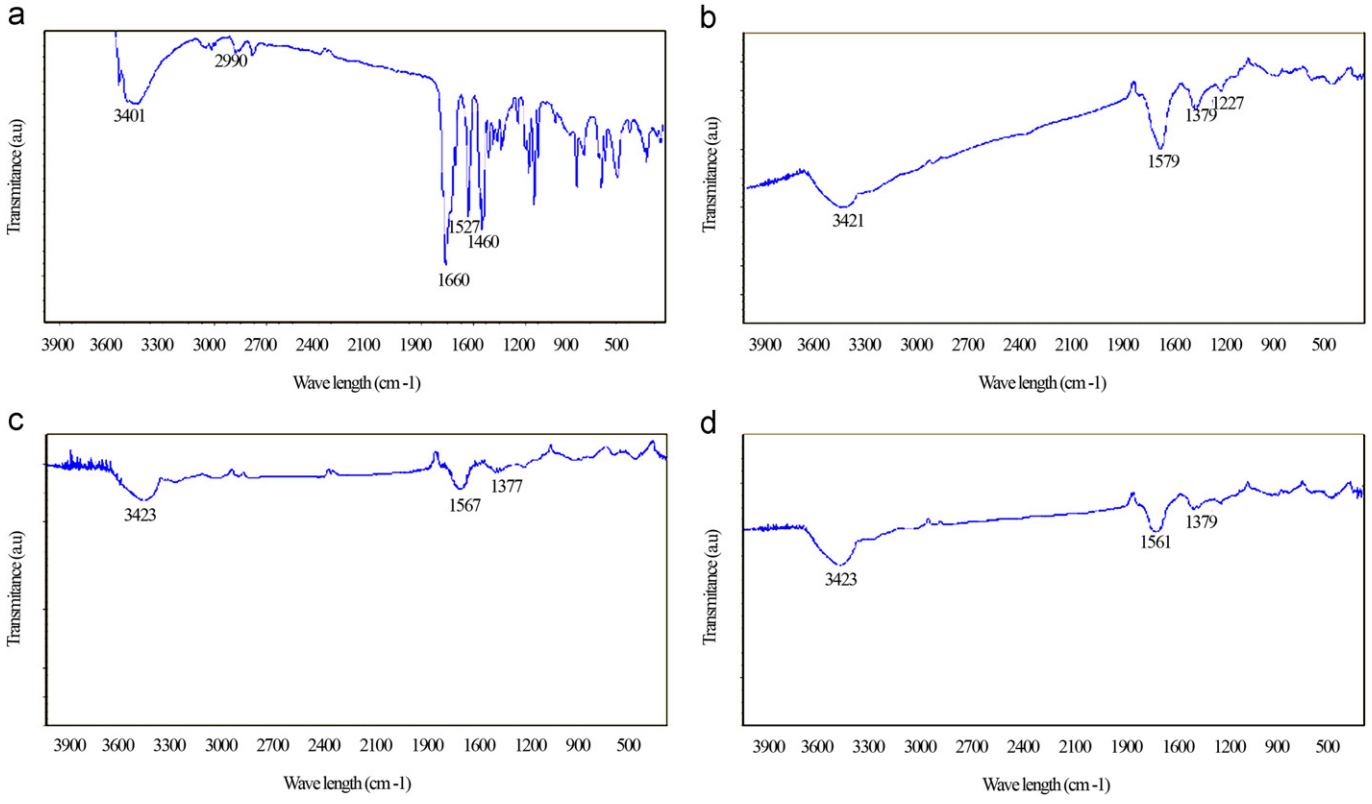


Fig. 5. FTIR spectra of (a) $Zn(Sal)_2$, (b–d) flower-like ZnS at different temperatures (b) 110 °C, (c) 140 °C, (d) 200 °C.

acid molecules and results in the fixed orientations of these thioglygolic acid molecules. In the IR spectra of ZnS precursors, the stretching vibrations at frequencies above 3000 $cm^{-1}$ were related to pure thioglycolic acid all shift toward the lower frequency, which might result from the chemical bonding action between $Zn^{2+}$ and S atom. In addition, at frequencies below 1600 $cm^{-1}$, the IR spectra of the ZnS obtained at 110–200 °C exhibit many differences from the pure thioglygolic acid, which should be due to the ordered alignment and regular conformation of thioglygolic acid molecules in the precursors. On the other hand, in liquid-state thioglygolic acid, the orientation and

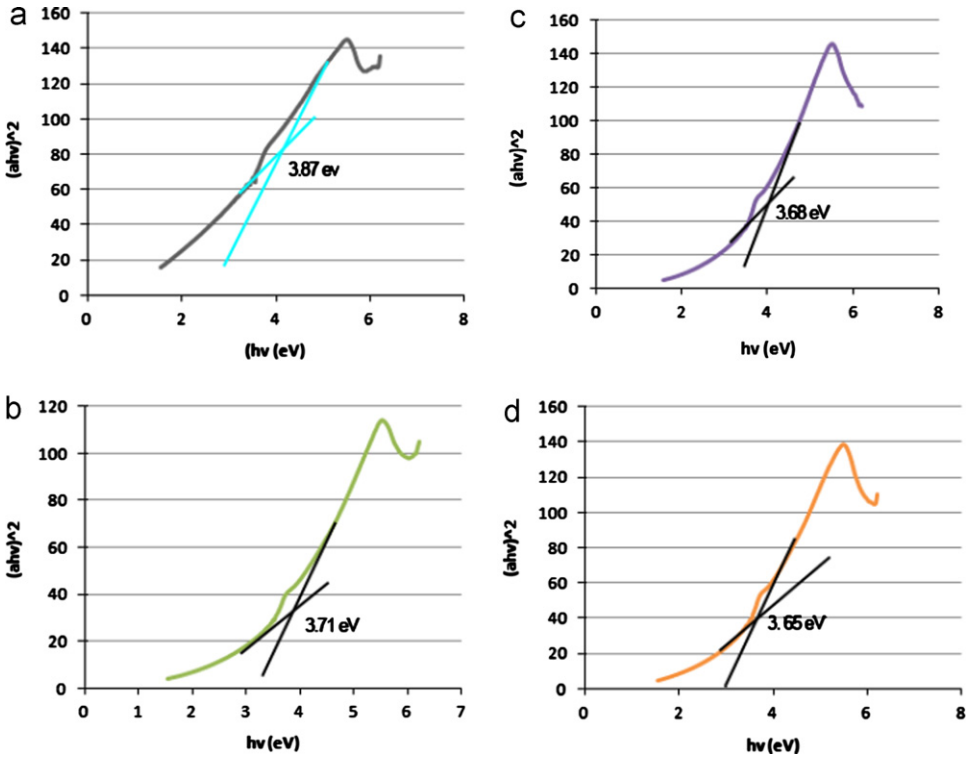


Fig. 6. Tauc plot of ZnS samples at different temperatures: (a) 110 °C (b) 140 °C (c) 160 °C and (d) 200 °C.

conformation of the molecules are randomized due to thermal perturbation. Also, at all samples, the bands at ~2350 $cm^{-1}$ are due to the presence $CO_2$ [8,16].

### 3.6. Optical properties of ZnS nanocrystals

In Fig. 6, the absorption shoulder is red shifted with increasing reaction temperature. This shows that crystals size is increased with the increase in reaction temperature. However, SEM images of the products show that there is no any considerable change in particle size of the nanosphere (Fig. 2a–h). But, by increasing the reaction temperatures from 110 °C to 200 °C, TEM, XRD and UV–vis absorption spectra clearly demonstrate considerable variation in the crystallite size of the products. The optical bandgap of ZnS nanosphere has been evaluated from the absorption spectrum using the Tauc relation [18–22]:

$$(\varepsilon h\nu) = C\left(h\nu - E_g\right)^n \tag{2}$$

where $C$ is a constant, $\varepsilon$ is the molar extinction coefficient, $E_g$ is the average bandgap of the material and $n$ depends on the type of transition. For $n=1/2$, $E_g$ in Eq. 2 is the direct allowed bandgap. The average bandgap, estimated from the linear portion of the $(\varepsilon h\upsilon)^2$ vs. $h\upsilon$ plots (Fig. 6), was found to decrease with increasing reaction temperatures from 110–200 °C. The bandgap values were higher than the value of bulk cubic zinc blende ZnS (3.72 eV) [23] due to quantum confinement of ZnS nanocrystals. The average particle size of ZnS nanocrystals was determined using Wang equation [24]

$$E_g = \left[E^2 + 2Eh^2\left(1/d_{abs}\right)^2/m^*\right]^{1/2} \tag{3}$$

where $E_g$ is the energy gap of ZnS nanocrystals, $E$ is the bandgap of bulk ZnS, and $d_{abs.}$ is the diameter of nanocrystals. The effective mass $m^*$ is defined as

$$\frac{1}{m^*} = \frac{1}{2}\left(\frac{1}{m_e} + \frac{1}{m_h}\right) \tag{4}$$

where $m_e$ is mass of electron and $m_h$ is mass of hole. For ZnS, $m_e$ and $m_h$ are reported to be 0.34 $m_0$, and 0.23 $m_0$ respectively, with $m_0$ being the rest mass of electron [25].

The bandgap values and the corresponding average particle size are listed in Table 2. The average crystallite size calculated was found to be in good agreement with XRD data (Table 1). This discrepancy in particle size is due to some approximations involved in the calculations. Neglecting the term containing permittivity in the Wang equation yields [26]:

$$E_g = E + \left(\hbar^2\pi^2/2R^2\right)\left(1/m_e + 1/m_h\right) - 1.786e^2/\rho R \tag{5}$$

where $R = d_{abs.}/2$, $p$ is the permittivity of nano ZnS and rest parameters have already been defined.

Fig. 6 shows the Tauc plot of the sphallerite ZnS nanoflowers prepared from hydrothermal method at different temperatures. As expected, the samples prepared at 110, 140, 160 °C (Fig. 6a–c) displayed excitonic absorption peaks at 320.40 nm (3.87 eV), 334.23 nm (3.71 eV) and 336.95 nm (3.68 eV), which had a blue shift of about 0.2, 0.03,

0.00 eV, respectively, as compared with the bandgap value (3.68 eV) of bulk cubic ZnS [17,23]. As expected, increasing reaction temperatures from 110 °C ($E_g = 3.87$ eV) to 200 °C ($\lambda_{abs.} = 339.72$ nm,3.65 eV) made a large red shift due to the crystal growth of as-prepared products. These results confirm the XRD data at Table 1. These phenomena were likely due to the quantum confinement effect of the as-synthesized ZnS nanocrystals [27], whose diameters are several nanometers, as shown in Fig. 3 and Table 1. This confinement effect can be clearly explained using the particle energy relation of the three dimensional single-particle box [27,28]:

$$E = A\left(\frac{{n_x}^2}{X^2} + \frac{{n_y}^2}{Y^2} + \frac{{n_z}^2}{Z^2}\right) \quad (6)$$

where $A$ is a constant; $n_x$, $n_y$, $n_z$ are the quantum number; $X$, $Y$, $Z$ are the scales in each dimension.

Apparently, a decreased $x$, $y$, $z$ value (the diameters of ZnS particles) leads to an increased energy $E$. The reduction of diameters of the particles produces a blue shift of the band edge. This is a good demonstration of the quantum confinement effect in the nanoparticles and other 0D nanostructure [28–33]. Another interesting property is its dielectric confinement effect. When organic molecules capped on semiconductor nanoparticles have a relatively smaller dielectric constant than that of the nanoparticles, the electric force lines emerging from charged particles within semiconductor nanoparticles pass through the surrounding medium; therefore, the screening effect is reduced and the Coulomb interaction between charged particles is enhanced. Such quantum confinement effects, as well as dielectric confinement effect, tailor the optical properties of semiconductor nanoparticles. Hence, it is critically important to synthesize the ZnS nanoparticles of a size comparable with Bohr radius and of a narrow size distribution in order to ensure the occurrence of these two effects [33]. Zinc sulfide has a low exciton Bohr radius (2.5 nm), making its nanoparticles interesting as small biomolecular probes for florescence and laser scanning microscopy. ZnS is also currently used as a shell or capping layers in core/shell nanoprobes such as CdSe/ZnS core/shell structures [15,33].

## 4. Conclusions

1. Sphalerite hierarchical ZnS nanocrystals have been successfully synthesized via a simple TGA assisted hydrothermally.
2. It has been found that the variations in reaction temperature up to 200 °C cannot have any significant effect on the shape and morphology of ZnS nanospheres.
3. The crystallite size of as-produced ZnS grows with increasing reaction temperatures from 110 °C to 200 °C.
4. The optical studies show that the absorption peaks of the TGA passivated ZnS nanoclusters are markedly blue shifted compared to those of the bulk ZnS, which clearly indicate the strong quantum size effect.
5. A mechanism for the formation of TGA encapsulated ZnS nanoclusters and thermal stability has also been suggested.
6. ZnS nanostructures with controlled synthesis have a high potential to scale-up for low-cost and large scale manufacturing of functional three dimensional nanomaterials, and open the door to a number of new applications.

## Acknowledgment

Authors are grateful to the council of Islamic Azad University, Kermanshah for providing financial support for this work. Two of the authors would like to present this work to their dear daughter, Sara, for her birthday. The authors also would like to thank Mr. Mahdavi, Dr. Abdi, Ms. Salehi, Mr. Tolui for conducting SAED, TEM, SEM analysis. The authors would also like to appreciate Mr. Emam Alizadeh and Mr. Adjabshiri for 2nd TEM series.

## References

[1] C. Feigl, S.P. Russo, A.S. Barnard, Safe, stable and effective nanotechnology: phase mapping of ZnS nanoparticles, Journal of Materials Chemistry 20 (2010) 4971–4980.
[2] X.S. Fang, C.H. Ye, L.D. Zhang, Y.H. Wang, Y.C. Wu, Temperature-controlled catalytic growth of ZnS nanostructures by the evaporation of ZnS nanopowders, Advanced Functional Materials 15 (2005) 63.
[3] N.S. Nirmala Jothi, P. Sagayaraj, The influence of capping by TGA and PVP in modifying the structural, morphological, optical and thermal properties of ZnS nanoparticles, Archives of Applied Science Research 4 (2012) 1079–1090.
[4] X. Fang, T. Zhai, U.K. Gautam, L. Li, L. Wu, Y. Bando, D. Golberg, ZnS nanostructures: From synthesis to applications, Progress in Materials Science 56 (2011) 175–287.
[5] L. Wang, L. Chen, T. Luo, Y. Qian, A hydrothermal method to prepare the spherical ZnS and flower-like CdS microcrystallites, Materials Letters 60 (2006) 3627–3630.
[6] L. Wang, J. Dai, X. Liu, Z. Zhu, X. Huang, P. Wu, Morphology-controlling synthesis of ZnS through a hydrothermal/solvthermal method, Ceramics International 38 (2012) 1873–1878.
[7] X. Wang, Q. Zhang, B. Zoua, A. Lei, P. Rena, Synthesis of Mn-doped ZnS architectures in ternary solution and their optical Properties, Applied Surface Science 257 (2011) 10898–10902.
[8] M. Salavati-Niasari, M.R. Loghman-Estarki, F. Davar, Controllable synthesis of wurtzite ZnS nanorods through simple hydrothermal method in the presence of thioglycolic acid, Journal of Alloys and Compounds 475 (2009) 782–788.
[9] H. Zhang, B. Chen, B. Gilbert, J.F. Banfield, Kinetically controlled formation of a novel nanoparticulate ZnS with mixed cubic and hexagonal stacking, Journal of Materials Chemistry 16 (2006) 249–254.
[10] X. Fang, Y. Bando, M. Liao, T. Zhai, U.K. Gautam, L. Li, Y. Koide, D. Golberg, An efficient way to assemble ZnS nanobelts as ultraviolet-light sensors with enhanced photocurrent and stability, Advanced Functional Materials 20 (2010) 500–508.
[11] X. Fang, Y. Bando, M. Liao, K.U. Gautam, C. Zhi, B. Dierre, B. Liu, T. Zhai, T. Sekiguchi, Y. Koide, D. Golberg, Single-crystalline ZnS nanobelts as ultraviolet-light sensors, Advanced Materials 21 (2009) 2034–2039.

[12] Z. Shen, G. Chen, Q. Wang, Y. Yu, C. Zhou, Y. Wang, Sonochemistry synthesis and enhanced photocatalytic $H_2$-production activity of nanocrystals embedded in CdS/ZnS/$In_2S_3$ microspheres, Nanoscale 4 (2012) 2010–2017.
[13] H. Zhang, D. Yang, X. Ma, D. Que, Some critical factors in the synthesis of CdS nanorods by hydrothermal process, Materials Letters 59 (2005) 3037–3041.
[14] C.L. Yan, D.F. Xue, Conversion of ZnO nanorod arrays into ZnO/ZnS nanocable and ZnS nanotube arrays via an in situ chemistry strategy, The Journal of Physical Chemistry B 110 (2006) 25850–25855.
[15] Y. Liu, G. Xi, S. Chen, X. Zhang, Y. Zhu, Y.T. Qian, New ZnS/organic composite nanoribbons: characterization, thermal stability and photoluminescence, Nanotechnology 18 (2007) 285605.
[16] M. Salavati-Niasari, M.R. Loghman-Estarki, F. Davar, Synthesis, thermal stability and photoluminescence of new CdS/organic composite hollow sphere nanostructures, Inorganica Chimica Acta 362 (2009) 3677–3683.
[17] M. Luo, Y. Liu, J. Hu, J. Li, J. Lui, R.M. Richards, General strategy for one-pot synthesis of metal sulfide hollow spheres with enhanced photocatalytic activity, Applied Catalysis B: Environmental 125 (2012) 180–188.
[18] F. Davar, M. Mohammadikish, M.R. Loghman-Estarki, Z. Hamidi, Synthesis of spherical ZnS based nanocrystals using thioglycolic assisted hydrothermal method, Crystal Engineering Communication 14 (2012) 7338–7344.
[19] L. Hu, J. Yan, M. Liao, H. Xiang, X. Gong, L. Zhang, X. Fang, Theoretical insight into faceted ZnS nanowires and nanotubes from interatomic potential and first-principles calculations, Journal of Physical Chemistry C 112 (2008) 4735–4742.
[20] A.E. Pop, V. Popescu, M. Danila, M.N. Batin, Optical properties of $Cu_xS$ nano-powders $Cu_xS$ ($x=1$–2), Chalcogenide Letters 8 (2011) 363–370.
[21] I. Moreels, K. Lambert, D. Smeets, D.D. Muynck, T. Nollet, J.C. Martins, F. Vanhaecke, A.′ Vantomme, C. Delerue, G. Allan, Z. Hens, ACS Nano 3 (2009) 3023–3030.
[22] K.S. Babu, C. Vijayan, R. Devanathan, Strong quantum confinement effects in polymer-based PbS nanostructures prepared by ion-exchange method, Materials Letters 58 (2004) 1223–1226.
[23] X. Fang, L. Wu, L. Hu, ZnS nanostructure arrays: a developing material star, Advanced Materials 23 (2011) 585–598.
[24] Y. Wang, A. Suna, W. Mahler, R. Kasowaki, PbS in polymers. From molecules to bulk solids, The Journal of Chemical Physics 87 (1987) 7315, http://dx.doi.org/10.1063/1.453325.
[25] S.K. Mehta, S. Kumar, S. Chaudhary, K.K. Bhasin, M. Gradzielski, Evolution of ZnS nanoparticles via facile CTAB aqueous micellar solution route: a study on controlling parameters, Nanoscale Research Letters 4 (2009) 17–28.
[26] Y. Wang, N. Herron, Nanometer-sized semiconductor clusters: materials synthesis, quantum size effects, and photophysical properties, The Journal of Physical Chemistry 95 (1991) 525, http://dx.doi.org/10.1021/j100155a009.
[27] J.Y. Zeng, Introduction to Quantum Mechanics, Peking University Press, Beijing, 1991.
[28] E.L. Wolf, Nanophysics and Nanotechnology: An Introduction to Modern Concepts in Nanoscience, Wiley-VCH, Weinheim, Germany, 2004, p. 63.
[29] M. Salavati-Niasari, F. Davar, M.R. Loghman-Estarki, Long chain polymer assisted synthesis of flower-like cadmium sulfide nanorods via hydrothermal process, Journal of Alloys and Compounds 481 (2009) 776–780.
[30] M. Salavati-Niasari, F. Davar, M.R. Loghman-Estarki, Controllable synthesis of thioglycolic acid capped $ZnS(Pn)_{0.5}$ nanotubes via simple aqueous solution route at low temperatures and conversion to wurtzite ZnS nanorods via thermal decompose of precursor, Journal of Alloys and Compounds 494 (2010) 199–204.
[31] C.L. Cowles, X. Zhu, N.G. Publicover, Fluorescence signal transduction mechanism for immunoassay based on zinc ion release from ZnS nanocrystals, The Analyst 136 (2011) 2975–2980.
[32] N.S. Nirmala Jothi, P. Sagayaraj, Archives of Applied Science Research 4 (2012) 1079–1090.
[33] Z. Jiang, H. Sun, Z. Qin, X. Jiao, D. Chen, Synthesis of novel ZnS nanocages utilizing ZIF-8 polyhedral template, Chemical Communications 48 (2012) 3620–3622.